An Online-Applicable Model for Predicting Health Degradation of PEM Fuel Cells With Root Cause Analysis

Taejin Kim, Hyunseok Oh, Hyunjae Kim, and Byeng D. Youn

***Abstract*—This paper proposes a new prognostic method for the health state of proton exchange membrane (PEM) fuel cells. The method is designed to predict the state-of-health (SOH) of PEMs and provide root cause analysis of the predicted health degradation. In this method, an equivalent circuit model (ECM) is built to emulate the impedance spectrum of PEM fuel cells. Because the key degradation parameters in the ECM cannot be measured *in situ*, this method instead estimates the parameters indirectly using the output voltage. The estimation is based on the linear relationship between the key ECM parameters and the output voltage. Using the constructed ECM and the estimated parameters, an impedance spectrum at the current moment is produced. The historical voltage evolution is then extrapolated using linear and exponential models that represent the irreversible and reversible phenomena, respectively. The models are used to predict future ECM parameters and, eventually, the impedance spectrum at any moment in the future. Through these steps, the proposed method provides an online estimation of the current SOH and predicts the level of future degradation. The primary novel feature of the proposed method is its ability to diagnose the root causes of potential degradation using data from nondisruptive online monitoring.**

***Index Terms*—Equivalent circuit model (ECM), fuel cells, impedance spectrum, state-of-health (SOH) prediction.**

I. Introduction

FUEL cells are promising candidates for future power generation because they are environmentally friendly and made from abundant resources. These advantages have led to the development of efficient fuel cells for possible uses in a variety of engineered systems, such as hybrid vehicles, aircraft, and smart grids [1]–[5]. However, commercialization of fuel cells remains a future prospect, rather than current reality, due to safety concerns. These concerns continue to delay widespread adoption of fuel cells in the field. Fuel cells are subject to degradation under normal operating conditions; however, excessive degradation of fuel cell components can trigger an explosion. Thus, accurate evaluation of the state of health (SOH) of fuel cells is necessary to enable condition-based maintenance to prevent eventual catastrophic failure.

Many researchers have attempted to develop an efficient method for estimating the health condition of fuel cells [6]–[10]. Most methods rely on machine learning techniques. Li *et al*. [6] showed a data-driven diagnosis method for proton exchange membrane (PEM) fuel cells that defines the relevant features and trains the classifier through the use of labeled data. A similar concept is also found in [11]. Other researchers showed that the model-based approaches use the voltage as a key feature for determining the degradation of fuel cells and developed black box models. For example, Marra *et al*. [7] used a neural network to estimate the voltage degradation in a solid oxide fuel cell. Silva *et al*. [8] improved the accuracy in estimating the voltage degradation through adaptive neuro-fuzzy inference. Jouin *et al*. [9] applied the particle filtering method to estimate the voltage degradation. Although voltage is often used to indicate the health condition of fuel cells, it only indicates the overall SOH of the entire fuel cell. In practice, performance degradation of each fuel cell component leads to degradation in the overall performance of a fuel cell system. Thus, while voltage reflects overall performance, it cannot distinguish the contributions of individual component from the overall degradation. There are other recently developed data-driven and model-based approaches available. For example, efficient real-time fault-tolerant control approaches [12], [13] and co-training method are developed for the data-driven method. Also, model-based methods are found in [14]–[17]. However, they are not yet applied to the fuel cell.

The impedance spectrum approach has received significant attention as an alternate way to diagnose fuel cell health. An impedance spectrum plot for fuel cells not only provides specific fault modes, but also indicates the contribution of individual components. A change of the impedance spectra corresponds to the degradation of a particular component of the fuel cell. This unique characteristic can potentially be exploited for fuel cell diagnosis [10], [18]. To this end, various equivalent circuit models (ECM) have been developed to aid in proper interpretation of the impedance spectrum [19]–[22]. However, obtaining an impedance spectrum plot through electrochemical impedance spectroscopy (EIS) requires stationary operating conditions and significant measurement time. Therefore, EIS is not practical for online use in real-world applications.

Manuscript received December 27, 2015; revised March 28, 2016; accepted April 11, 2016. Date of publication June 29, 2016; date of current version October 7, 2016. This work was supported in part by the Mid-Career Researcher Program (NRF-2013R1A2A2A01068627) through the National Research Foundation of Korea funded by the Ministry of Science, Information and Communications Technology, and Future Planning and in part by the Institute of Advanced Machinery and Design, Seoul National University.

The authors are with the Department of the Mechanical Engineering, Seoul National University, Seoul 08826, South Korea (e-mail: godori16@snu.ac.kr; hyunseok52@gmail.com; secutus07@snu.ac.kr; bdyoun@snu.ac.kr).

Color versions of one or more of the figures in this paper are available online at http://ieeexplore.ieee.org.

Digital Object Identifier 10.1109/TIE.2016.2586022

More recently, broadband current interruption techniques have been developed to overcome the limitations of the traditional EIS techniques. These methods impose current interrupting waveforms on the operating current, such as pseudo-random binary sequence, multisine signals, and optimized broadband signals [23]–[25]. These methods estimate the impedance spectrum by analyzing the response of the voltage to the interrupting current. The methods reduce the measurement time and extract information similar to that found through EIS measurements. However, these methods still require specialized equipment, such as impedance analyzers. Moreover, when current interruption methods are used in practical settings, repeated measurements are needed to increase accuracy [25]–[27]. This requirement limits the usefulness of these methods since, during the measurement activity, the superposition of multiple waveforms interrupts the operation of the fuel cell [23].

In this paper, we propose an ECM approach that can diagnose a fuel cell's current SOH and predict its future SOH. In our method, the impedance spectrum is modeled using an ECM approach. To demonstrate our method, two PEM fuel cell stacks were tested under stationary current and rippled-current conditions, while maintaining other conditions constant. We estimated and predicted the ECM parameters of the stacks at particular times using the online-measurable voltage. Our proposed method allows determination of the impedance spectrum in real time or at any desired time, without any extra equipment. In addition, changes in the ECM parameters—estimated using the physical quantity—enable the method to be used to indicate the physical root causes of the health degradation observed.

The rest of this paper is organized as follows. The experimental setup and data acquisition method are described in Section II. In Section III, the ECM is described as our proposed way to model the impedance spectra. Section IV explains the method for estimation of ECM parameters in conjunction with the construction of the impedance spectra. The estimated parameters are then interpreted to represent the physical degradation inside the fuel cell. For the purpose of SOH prediction, however, the voltage cannot be measured; instead, it must be predicted. The voltage prediction procedure is described in Section V. Finally, Section VI provides the results of the suggested algorithm and a concluding discussion.

II. Experimental Setup

In Section II-A, the principles of the fuel cell that includes the structure, working principles, and the causes and effects of degradation are briefly explained. Section II-B describes experiments that were conducted to understand the degradation behavior and to set up the proposed health diagnostic strategy.

A. Principles of PEM Fuel Cells

The basic structure of a PEM fuel cell contains an anode, a cathode, and electrolyte. Hydrogen is supplied from the anode side. It reacts with the oxygen coming from the cathode side, and, as a result, makes water. This overall reaction is made up of two reactions

$$\mathrm{H_2} \rightarrow 2\mathrm{H^+} + 2\mathrm{e^-}$$
$$\frac{1}{2}\mathrm{O_2} + 2\mathrm{H^+} + 2\mathrm{e^-} \rightarrow \mathrm{H_2O}.$$

The first reaction, separation of a hydrogen molecule into hydrogen ions and electrons, occurs at the interface between the anode and the electrolyte. The hydrogen ions then move to the cathode through the electrolyte to complete the reaction. Since the electrolyte only allows the ions to pass, the electrons transfer through an external wire and provide energy to the load on the way to the cathode. This process continues as long as the hydrogen fuel supply remains. Most fuel cells use the same or a similar working process; they are differentiated by their choice of electrolyte. The PEM fuel cells used in this research contain a polymer membrane that provides high power density at a low operating temperature.

Each individual component of a PEM fuel cell degrades during operation. The degradation rate slows down during particular working steps, such as during the transportation of the reactants and during charge transfers. It also varies based on the rate of the electrochemical reactions. The variation in fuel cells' degradation rates is due to the varied rates of the degradation of each individual component in the fuel cell: membrane, catalyst layer, gas diffusion layer, and bipolar plates [28]. The membrane can undergo mechanical, thermal, and electrochemical degradation. Nonuniform stresses during the assembly or cycling hydration induce mechanical stress on the membrane. Reactant crossover via pinholes and/or perforations increases operating temperature, which in turn decomposes the membrane. Also, the radicals generated by the undesirable side reaction diminish the membrane. In the electrocatalyst layer, the detachment, dissolution of the catalyst, and growth in the catalyst particle reduce the catalytic area and, thus, reduce catalyst activity [29]. Also, corrosion can occur in the gas diffusion layer and on the bipolar plates. Degradation of individual components, of course, occurs in a combined manner. For example, the electrochemical side reaction weakens the mechanical strength of the membrane.

B. Data Description

The experiment of interest was conducted by FCLAB—The Federation for Fuel Cell Research (FR CNRS 3539)—for the 2014 IEEE PHM Data Challenge Competition. Details of the experiment are available in [30]. This section provides an overview of only the PEM fuel cell experiments that are relevant to the development of the proposed method. For the test, the PEM fuel cell stacks with five cells, Type BZ 100 built by the Ulmer fuel cell manufacturer were used. The membrane electrode assemblies of the cells consist of Gore Primea 5761 membranes and SGL 10 BB graphite paper as gas diffusion layers. The active area of a single cell was 100 cm^2. The nominal current density and the maximal current density of the cell were 0.70 and 1 $\mathrm{A/cm}^2$, respectively. The maximum available power for the whole stack was 600 W. Two stacks were aged under different operating conditions. The first stack, called "FC1," operated

TABLE I
CHARACTERIZATION TEST SCHEME

	Characterization tests	Training conditions
FC1	1. Polarization curve	Test time (hours)
	2. EIS after polarization	0, 48, 185, 348, 515, 658, 823, 991
		Current density: 0.70 A·cm^{-2} (for polarization test)
		Current density: 0.70 A·cm^{-2} (for EIS test)
FC2	1. Polarization curve	Test time (hours)
	2. EIS after polarization	0, 35, 182, 343, 515, 666, 830, 1016
		Current density: 0.70 A·cm^{-2} (for EIS test)

under a nominal current condition, 0.7 A/cm^2. The second stack, "FC2," was tested under a rippled current condition: 0.7-A/cm^2 current density with 10% oscillation at a frequency of 5 kHz. In addition to the current conditions, several physical parameters were controlled and others were measured. The inlet air was heated to about 42 °C, relative humidity was 50%, and the inlet pressure of both sides was kept at 1280 mbar. For inlet hydrogen, the relative humidity and the temperature were measured at their ambient conditions.

During the aging tests, polarization curves and EIS were measured intermittently (roughly every week) to check the SOH of the PEM fuel cells. As shown in Table I, for both FC1 and FC2, the EIS tests were conducted after the polarization tests, with a current density of 0.70 A/cm^2 and a frequency range from 10 mHz to 50 kHz. The voltage was measured constantly during the entire aging test.

III. DEVELOPMENT OF ECM FOR PEM FUEL CELLS

The outcome from EIS testing, the impedance spectrum, is considered an indicator of the overall health of a PEM fuel cell. The SOH is inferred by relating the characteristics of the impedance spectrum to the fuel cell's health. ECM helps define the links between the characteristics of the impedance spectrum and the fuel cell's health. An ECM combines basic circuit elements to represent the electrical behavior of a given circuit. In this case, the ECM is a model of the overall fuel cell. The values of basic circuit elements, such as resistance, inductance, or capacitance, are themselves used as health indicators.

The typical impedance spectrum of a fuel cell contains three overlapping semicircles representing the anode activation loss, the cathode activation loss, and the mass transport loss in the fuel cell. The impedance spectrum in this study is shown in Fig. 1(a). There are two semicircles—one at high frequency and one at low frequency—that correspond to the cathode activation loss and the mass transport loss, respectively. The anode activation loss is not seen in the figure because it is covered by the semicircle of the cathode activation loss. This is often the case because the hydrogen oxidation reaction at the anode is greater than the oxygen reduction reaction at the cathode.

A semicircle with a perfectly round shape was modeled using a parallel connection of a resistor and a capacitor, as shown in Fig. 1(b). In the high-frequency semicircle, a resistor—called a Faradaic resistor—demonstrates the reaction kinetics, and a capacitor shows the capacitance effect caused by the charge

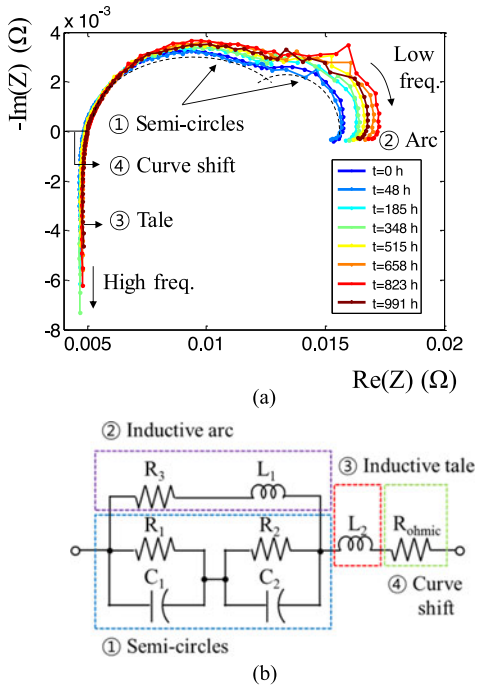

Fig. 1. (a) Impedance spectrum plot of the tested PEM fuel cells (FC1) and (b) corresponding ECM.

separation at the interface of the electrode and the membrane. In the low-frequency semicircle, a resistor can be used to reflect the mass transport resistance. However, the semicircles displayed in Fig. 1(a) are not perfectly circular, i.e., they are partially depressed. This depression is caused by the nonhomogeneous distribution of electron charges inside the porous electrode [31]. Prior work has demonstrated that the constant phase element (CPE), rather than the standard plane capacitor, represents the depression sufficiently [24]. The impedance of the CPE is shown as follows:

$$Z_{\mathrm{CPE}} = \frac{1}{C(i \cdot w)^k} \tag{1}$$

where w is the angular frequency, C is the factor of proportionality, and k is the CPE exponent that characterizes the phase shift. The CPE exponent rotates the complete semicircle by $90°(1-k)$ and makes the circle depressed. Next, the cathode is modeled using the parallel connection of a Faradaic resistor R_1 and the CPE C_1. For mass transport modeling, the Warburg impedance is widely used, but, in this paper, an *R*//CPE parallel circuit replaces the Warburg impedance because it requires less parameters but shows clear relationship with the voltage and still explains the overall phenomenon of the mass transport. However, if more specific or accurate interpretation is required, one can use the Warburg impedance or a series of R//CPE circuits. Here, the mass transport resistor R_2 and another CPE C_2 are connected in parallel to represent the mass transport phenomenon. Then, the overall impedance is obtained by connecting the parallel circuits in series. Then, the total impedance of the electrodes is

$$Z_1 = \frac{1}{R_1^{-1} + C_1(iw)^{n_1}} + \frac{1}{R_2^{-1} + C_2(iw)^{n_2}}. \tag{2}$$

The PEM fuel cells used in this research show two additional characteristics: the arc at the low-frequency end and the tail at the high-frequency end—both below the real axis. The arc in the low frequency is caused by the inductive effect. Possible explanations of this inductive effect are found in the literature. For example, several studies [18], [32], [33] have indicated that hydrogen peroxide intermediate is associated with the inductive effect during the oxygen reduction reaction at the cathode. Roy *et al*. [33] also suggested that the loss of catalytic activity due to platinum dissolution can be related to the low-frequency inductive loop. In addition, carbon monoxide poisoning and water transport problems were pointed out as possible reasons for the inductive effect [24], [26].

The inductive effect at low frequency is modeled by adding an *R–L* circuit on both reaction kinetics and mass transport *R//C* circuits. Then, the *R–L* circuit can explain both of the side reactions, for example, through the formation of hydrogen peroxide, carbon monoxide poisoning, or the mass-transport-related inductive effect. Then, the impedance is calculated as follows:

$$Z_{\mathrm{LF}} = \frac{1}{{Z_1}^{-1} + (R_3 + iwL_1)^{-1}}. \tag{3}$$

Although it rarely happens, some researchers have reported that the long tail at high frequency can also be caused by an inductive effect. The high-frequency inductive behavior is mainly associated with connecting elements, such as external wires, to fuel cells [34]. Thus, it can be modeled simply by imitating an external wire with an inductor L_2 and a resistor. The ohmic resistor for the external wire is included in the fuel cell's total ohmic resistance. Then, the ECM becomes

$$Z_{\mathrm{HF}} = \frac{1}{{Z_1}^{-1} + (R_3 + iwL_1)^{-1}} + iwL_2. \tag{4}$$

Finally, the amount that the curve shifts from the origin indicates the magnitude of the ohmic resistance of the fuel cell stack. The ohmic resistance consists of several resistances of the components, including the membrane, catalyst layer, contact resistance between components, and the external wires. Among these resistances, the membrane resistance is the most significant contributor to the ohmic resistance [24]. For the ECM, this ohmic resistance is modeled by serially connecting the resistor R_{ohmic} to the rest of the circuit. By adding the ohmic resistor to (4), the completed circuit model is given [as shown in Fig. 1(b)] and the corresponding impedance is calculated as follows:

$$Z = \frac{1}{{Z_1}^{-1} + (R_3 + iwL_1)^{-1}} + iwL_2 + R_{\mathrm{ohmic}}. \tag{5}$$

The parameters and the possible root causes are summarized in Table II. By obtaining the parameters, the root causes of the degradation of the fuel cell can be predicted. This prediction is described in the following sections.

TABLE II
CAUSES OF PARAMETER CHANGE

Parameters	Root causes of parameter change
L_1, R_3	Byproduct formation (peroxide, hydrogen peroxide, carbon monoxide, etc.)
	Platinum dissolution
	Degenerated mass transport
L_2	External wire setup
C_1, C_2	Catalyst loss
R_{ohmic}	Chemical attack by radicals
	Thermal decomposition of the membrane
	Dehydration of the membrane
R_1	CO poisoning
	Catalyst degradation
	Agglomeration of the catalyst
	Corrosion of the catalyst carbon support
R_2	Flooded gas diffusion layer
	Carbon corrosion (affecting mass transport)

IV. VOLTAGE-BASED ESTIMATION OF IMPEDANCE SPECTRA

Diagnosis of the state of health of PEM fuel cells can be conducted by estimating the impedance spectra or parameters of the relevant ECM. However, neither the impedance spectrum nor the ECM parameters for PEM fuel cells are measurable during operation. Thus, to enable the use of this method in practical settings, the impedance spectra or parameters need to be estimated from online-measurable quantities. Several studies have been conducted to obtain information about fuel cell degradation using online-measurable quantities [7], [9]. These studies used the voltage as both a measurable quantity and as a health indicator itself. Although voltage is a good health indicator, it only describes overall health of the fuel cell. Voltage contains limited information on the health status of individual fuel cell components. In contrast, the impedance spectrum allows more robust information to be inferred about the health of individual components. Therefore, in this study, we investigate a diagnostic method that offers online applicability (using voltage) and detailed health status (provided by the impedance spectrum). Our work examines the relationship between the voltage and the ECM parameters.

The output voltage is expressed as the thermodynamic potential with several losses subtracted

$$V = E_{\mathrm{thermo}} - \eta_{\mathrm{ohmic}} - \eta_{\mathrm{act}} - \eta_{\mathrm{conc}} \tag{6}$$

where E_{thermo} is the thermodynamic maximum potential of the fuel cell and η_{ohmic}, η_{act}, and η_{conc} are the ohmic loss, activation loss, and concentration loss of the fuel cell, respectively. The losses are affected by the performance and degradation of the fuel cell components. Thus, they can be expressed as a function of the ECM parameters that also represent the fuel cell components. For example, the ohmic loss that occurs due to charge transfer impedance is expressed as follows:

$$\eta_{\mathrm{ohmic}} = iR_{\mathrm{ohmic}} \tag{7}$$

where i is the current density that flows between the electrodes and R_{ohmic} is the combined ohmic resistance of the fuel cell, which is the same as that used in (5) for the ECM. From (6) and (7), we know that a change of external voltage occurs if the ohmic resistance is changed by the degradation of the charge transfer conductor. Moreover, the change is inversely proportional to the change of the ohmic resistance. It is known that the ohmic resistance is mainly affected by the water content

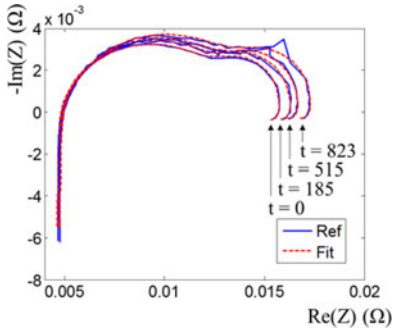

Fig. 2. ECM fitting result with four parameters.

and the temperature of the membrane. In this study, we assume that the change of the ohmic resistance due to the relative humidity and the temperature is minimized by the constantly controlled humidification of the air and the consistently controlled temperature [35].

Similar to the ohmic loss, the activation loss is related to the ECM parameters, expressed in the Tafel equation

$$\eta_{\text{act}} = -\frac{RT}{\alpha n F}\ln j_0 + \frac{RT}{\alpha n F}\ln j = a + b\log j \tag{8}$$

where R is the ideal gas constant; T is the temperature; α is the transfer coefficient; n is the number of electrons; F is the Faraday constant; and j and j_0 are the input current density and the exchange current density, respectively. In (8), it is assumed that the activation loss is dependent on the exchange current density, while other parameters, including the temperature and input current density are set to be constant. The exchange current density is also expressed as follows [35]:

$$j_0 = \left(\frac{RT}{\alpha n F}\right)\frac{1}{R_f e^{\alpha n F \eta_{\text{act}}/(RT)}} \tag{9}$$

where R_{f} is the Faradaic resistance corresponding to R_2 in the developed ECM of (2) and (3). As seen in (9), the Faradaic resistance is related by the log function to the activation loss. However, in this study, it is modeled using the linear function. It is reasonable to assume a linear relationship for the small changes of Faradaic resistance; thus, this strategy prevents exponential divergence due to errors in parameter estimation. The assumption also helps map the ECM parameters and the voltage independently. R_1, which is related to the concentration loss, is estimated in the same way due to the symmetry with R_2. Although R_3 results from the by-product of the side reaction, we assume that R_3 also has a linear relationship with voltage, considering R_3 as a contaminant that blocks the active sites of the catalyst [36]. Based on the above discussion, as an example, the impedance spectra of FC1 at 658, 823, and 991 h can be estimated. To achieve this goal, first, the impedance spectrum before the estimation time is assumed to be known; thus, the corresponding ECM parameters are also assumed to be known. Then, to estimate the ECM parameters at given times, the functions between the voltage and the ECM parameters are empirically constructed, as described earlier. Before the development of the relationship, the negligible parameters, of which values seldom change during the aging process, are first

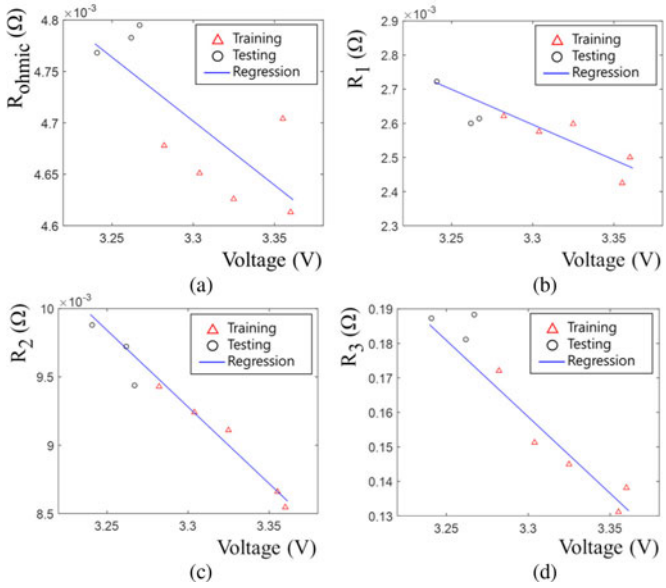

Fig. 3. Linearity between voltage and ECM parameter (a) R_{ohmic}, (b) R_1, (c) R_2, and (d) R_3.

TABLE III
ESTIMATED ECM PARAMETERS

ECM Parameters	$t = 658\,h$	$t = 823\,h$	$t = 991\,h$
$R_{\text{ohmic}} = -0.0012\,V + 0.0088\,\Omega$	4.77×10^{-3}	4.75×10^{-3}	4.74×10^{-3}
$R_1 = -0.0021\,V + 0.0094\,\Omega$	0.0027	0.0027	0.0027
$R_2 = -0.0112\,V + 0.0463\,\Omega$	0.0097	0.0099	0.0097
$R_3 = -0.4434\,V + 1.622\,\Omega$	0.1755	0.1849	0.1733

fixed to their mean values. In the literature, the capacitance, the inductance, and the CPE components are pointed out as degradation-irrelevant parameters for given operating conditions [34]. Consequently, the parameters C_1, C_2, L_1, L_2, n_1, and n_2 are fixed to their mean values from the training data set. This reduction in the number of estimation parameters keeps the accuracy, while providing the advantage of preventing overfitting to the measured data that could occur with the inclusion of such degradation-irrelevant parameters. After fixing those values, the rest of the parameters R_{ohmic}, R_1, R_2, and R_3 are then recalculated by curve fitting. Fig. 2 shows the curve fitting results for the four parameters. The average root mean square error is 2.9127×10^{-4} for the four parameters.

As shown in Fig. 3, the recalculated parameters were used to find the relationship between the voltage and the parameters. The red triangles are the training data points and the blue linear line shows the results of the curve fitting of the training data points. The black circles are the fitted parameters, that is, the parameters at the testing data points: 658, 823, and 991 h. These values are estimated by the blue line, using the voltages at the testing times. Visual inspection of the plots confirms that the regression curves properly represent the relationship between the voltage and the parameters.

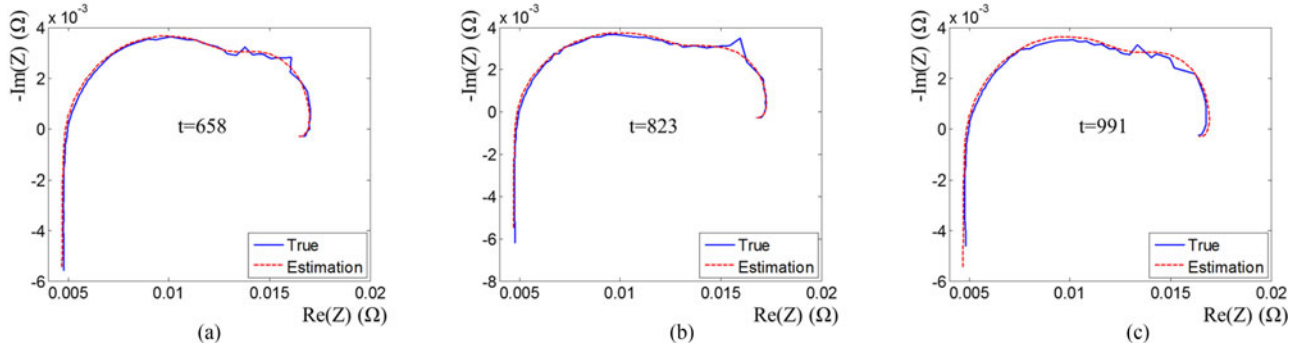

Fig. 4. Estimated impedance spectrum results of FC1 at time (a) 658, (b) 823, and (c) 991 h.

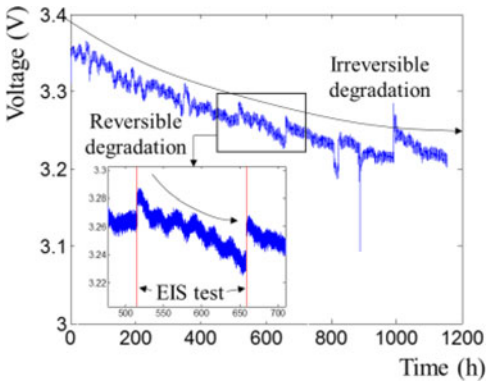

Fig. 5. Irreversible and reversible voltage degradation.

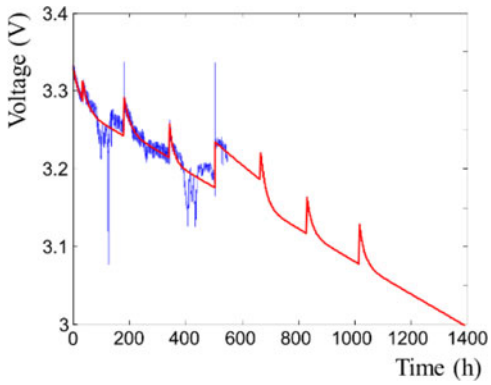

Fig. 6. Comparison of the predicted voltage degradation (red line) to the measured voltage (blue line) for FC2.

The linear behavior of R_{ohmic} and the voltage can be explained using (1) and (2). From the equations, we can see that an increase in ohmic resistance results in a decrease in voltage. For R_1, the impedance of the electrode is $Z = 1/(R_1^{-1} + jwC_1)$, so for a fixed value of C_1, R_1 is linear with Z when $R_1 << C_1$. Thus, again the voltage loss at electrode $V = iZ$ is proportional to R_1. Similar explanations are possible for R_2 and R_3. The parameters are estimated separately from the voltage values because they are all linear. The curve fitting parameters, a and b, as in $aV + b$, and the estimated parameters, R_{ohmic}, R_1, R_2, and R_3, are shown in Fig. 3 and Table III. This relationship, plus the voltages obtained at 658, 823, and 991 h, gives the ECM parameters for each time of interest and thus the impedance spectra. The impedance plots based on the estimated ECM parameters are plotted in Fig. 4. The uncertainty can be realized in the form of the residual between the data and the linear fitting in Fig. 3. The standard deviations of R_{ohmic}, R_1, R_2, and R_3 are 2.07×10^{-5}, 2.57×10^{-5}, 7.04×10^{-5}, and 4×10^{-3}, respectively. Given a 95% confidence interval for each parameter, the root mean squares errors between the estimated and the measured impedance spectrum at 823 h are increased by 0.03%, 0.11%, 0.51%, and 0.04%. Note that the residual of R_{ohmic} seems to have large variation. This does not affect much to the estimation results because the sensitivity or slope of the linear fitting is not large. The residuals of other parameters are accurately estimated in a relative sense, compared to their sensitivity.

TABLE IV
PREDICTED ECM PARAMETERS

	$t = 0\,h$	$t = 666\,h$	$t = 830\,h$	$t = 1016\,h$	Related Root Causes
R_{ohmic}	0.0044	0.0045	0.0045	0.0046	Membrane degradation
R_1	0.0027	0.0029	0.0030	0.0031	Loss of cathode activation
R_2	0.0088	0.0104	0.0105	0.0117	Mass transport resistance
R_3	0.1339	0.1991	0.2054	0.2553	Radical formation

V. VOLTAGE-BASED PREDICTION OF THE IMPEDANCE SPECTRUM

Prediction of the impedance spectrum for PEM fuel cells is challenging because no online measurement data are available for a particular time in the future. Estimation of the impedance spectra cannot be directly implemented without this future voltage information. Thus, first, future voltage information needs to be predicted.

Voltage shows two different degradation behaviors, irreversible and reversible degradation [37], [38]. Permanent damage to the fuel cell components by physiochemical reactions (such as corrosion or membrane degradation) results in irreversible phenomena, whereas temporary disruption of the fuel cell performance (such as poisoning of the anode catalyst by carbon monoxide, membrane drying, or cathode flooding) leads to reversible degradation [37]. As an example, in Fig. 5, the voltage of FC1 shows the two degradation patterns. The overall voltage

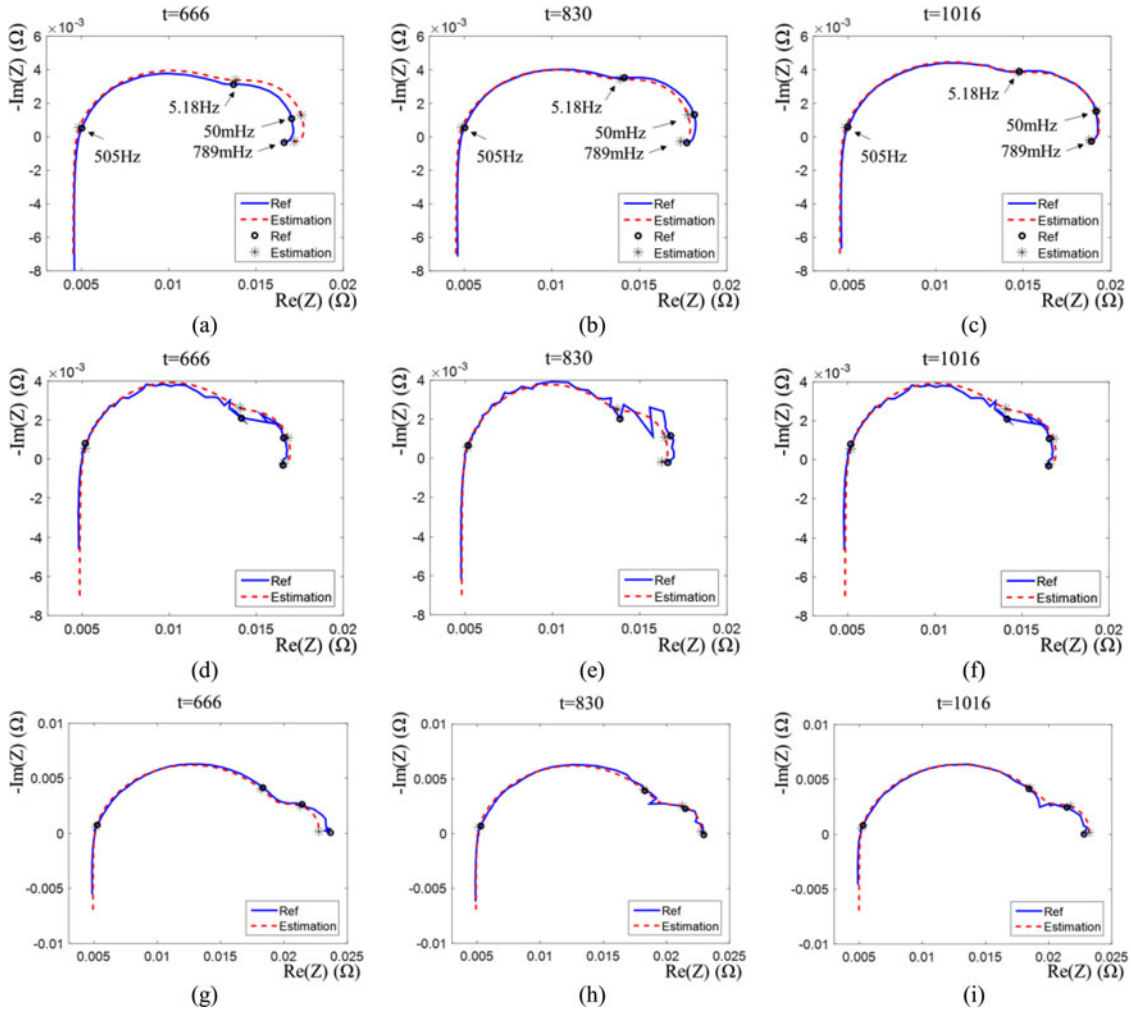

Fig. 7. Predicted impedance spectrum results of FC2; with 75-A current at time (a) 666, (b) 830, and (c) 1016 h; with 45 A current at time (d) 666, (e) 830, and (f) 1016 h; and with 20-A current at time (g) 666, (h) 830, and (i) 1016 h.

decrease indicates irreversible degradation, while the temporary recovery of the voltage after the EIS test shows reversible degradation. The irreversible voltage degradation that occurs under constant operating conditions can be modeled using a linear model [9]. For reversible voltage degradation, an exponential model can appropriately model the degradation [38].

By fitting a linear model to the voltage degradation data of FC1, the irreversible degradation rate is found to be –0.1959 mV/h; this is also used to represent the degradation rate of FC2. Although the voltage degradation rate under a rippled current is generally greater than that under a constant current, it has been reported that a 10% ripple does not affect the degradation rate significantly [39]. With this in mind, the reversible voltage loss can be calculated as the difference between the voltage degradation and the irreversible voltage loss. It can be described by the exponential model, $a\times\exp(b\cdot t)+c$. The exponential model is fitted to the reversible voltage loss of FC2 for the given data up to 550 h. After this time, the exponential parameters are found based on the information about FC1. The parameter a in the exponential model is simply the last value of the voltage before the EIS test. The decay rate b is found by calculating the mean value of the previous decay rates of FC2. The amount of voltage recovery, parameter c, is obtained from the value of FC1. Fig. 6 illustrates the result of the predicted voltage degradation model with both reversible and irreversible degradation processes.

For FC2, the relationship between the voltage and the four ECM parameters at 0, 35, 182, 343, and 515 h was developed using the process described in Section IV. Then, the ECM parameters for a specific future time are obtained from the predicted voltages, which are shown in Table IV, and the impedance spectra are reproduced using the ECM and its predicted parameters. Fig. 7 illustrates the corresponding impedance spectra plots at 666, 830, and 1016 h. Results from a second experiment using the same method under a different current density are also shown.

According to the results in Table IV, all the parameters increase through time except R_{ohmic}, which remains nearly constant. In particular, R_3 increases to double its initial value. This indicates that the major root cause of the performance degradation is the formed radicals. In addition, R_1 and R_2 increase by about 15% and 33%, respectively. This implies that the performance of the PEM fuel cell under study is partially degraded due to the electrodes.

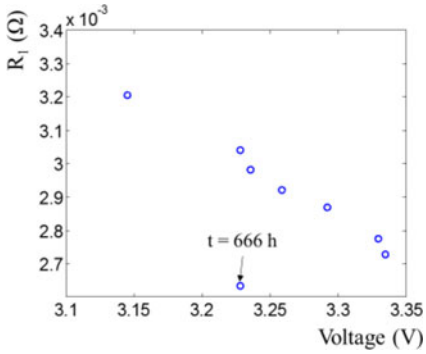

Fig. 8. Off-trend of ECM parameter *R*1 at 666 h.

Three measures have been defined to quantify the accuracy of this method [30]. In (10), the accuracy of the prediction is first obtained based on the Euclidean distance between measured and predicted impedances at four different frequencies, 50 mHz, 789 mHz, 5.18 Hz, and 505 Hz ($\mathrm{ED}_{\mathrm{Fr}/t}$). The calculated Euclidean distances at 666, 830, and 1016 h are weighted according to their distance from 550 h and summed to Err_t as in (11). Then, the average of the weighted-sum error gives the final score $\mathrm{Score}_{\mathrm{SOH}}$ in (12)

$$\mathrm{ED}_{\mathrm{Fr}/t} = \sqrt{\left(\mathrm{Re}(Z_{\mathrm{Fr}/t}) - \mathrm{Re}(\hat{Z}_{\mathrm{Fr}/t})\right)^2 + \left(\mathrm{Im}(Z_{\mathrm{Fr}/t}) - \mathrm{Im}(\hat{Z}_{\mathrm{Fr}/t})\right)^2} \tag{10}$$

$$\mathrm{Err}_t = \frac{1}{t - 550} \sum_{\mathrm{Fr}} (\mathrm{ED}_{\mathrm{Fr}/t}) \tag{11}$$

$$\mathrm{Score}_{\mathrm{SOH}} = \frac{1}{3} \sum_{t} (\mathrm{Err}_t). \tag{12}$$

In this study, the score of the suggested method is 5.32×10^{-6}, which is a better score than that provided by the state-of-the-art method reported in the 2014 PHM Data Challenge Competition (i.e., regression analysis with "leave-one-out" scoring 7.89×10^{-6} [40]). We also conducted predictions using machine-learning-based techniques, specifically, the artificial neural networks and relevance vector machine. The training data contain the ECM parameters for all relevant times for FC1 and the ECM parameters at the first five times of FC2. The test dataset is the last three ECM parameters of FC2. The scores of the algorithms are 1.07×10^{-5} and 1.34×10^{-5}, respectively. For the machine learning method to be effective, a significant amount of data must be available. Here, enough data are not available; thus, the physics-based method shows a better result.

The error in the predicted results comes primarily from two sources. The first error source is the uncertainty in the ECM parameter estimation that results from the linear regression function. Some level of noise is involved in estimating the linear relationship between the ECM parameters and voltage. This error is dominant for the estimation of R_1 at 666 h, as shown in Fig. 8. The size of the second semicircle that is determined by R_1 shows a larger prediction error than the other instances. We believe that this trend is caused by a greater level of voltage noise. This can also be found at around 100 h and 420 h in FC2 (see Fig. 6). The second error source is uncertainty in the voltage prediction model. The suggested voltage prediction model uses assumptions that simplify the problem, such as the amount of voltage jump after the characterization test. These uncertainties need to be addressed in the future. Furthermore, this study uses only voltage information for SOH prediction; however, the use of other measurements (e.g., EIS tests with different currents or polarization curves) can lead to better results.

VI. Conclusion

This paper proposed a new method for health prognostics of PEM fuel cells. The proposed method consists of the following:

1) modeling an ECM that emulates the impedance spectrum of the fuel cells;
2) estimating the parameters of the ECM using voltage measurements;
3) predicting the future health condition of the fuel cells by extrapolating the voltage degradation trend; and
4) analyzing root causes of the degradation of the fuel cells by predicting future values of the ECM parameters.

Using the proposed technique, the future SOH of fuel cells can be predicted online and with root cause analysis. The prediction accuracy of the proposed method outperformed the state-of-the-art method that was previously reported (i.e., regression analysis using the "leave-one-out" method).

Each existing online-prognostic method for fuel cells has limitations in practical applications. While broadband current injection techniques were recently proposed to overcome the limitations of the classical EIS techniques, they require 1) extra equipment to diagnose the fuel cells and 2) a lengthy measurement time to achieve accurate characterization. Voltage-based prognostic methods provide the SOH of the overall system; however, they lack the ability to identify the degradation of individual components (electrodes, membrane, etc.) in the fuel cells. Unlike the voltage-based methods, use of the impedance spectrum provides information about the SOH of individual components in the fuel cell; however, the measurement of impedance spectra has to be conducted under stable loading conditions. This study attempted to combine the merits of two methods (i.e., the broadband current injection technique and the impedance spectrum measurement technique). The proposed method has two main advantages over existing methods: 1) it can predict the future SOH of PEM fuel cells using data available through online monitoring and 2) it can identify the root causes of expected future failure. As a result, the root causes of fuel cell degradation, namely, membrane degradation, cathode degradation, and the mass transport problem, can be predicted during the operation.

In this study, training data are obtained under almost constant current condition. This condition is believed to be relevant to many of the fuel cell applications, since the fuel cell is suitable to supply stable power rather than highly dynamic power. Furthermore, based on this test condition, it was assumed that there are linear relationships between the ECM parameters and the voltage. However, this assumption may not be true for PEM

fuel cells that are subjected to dynamic operating conditions, including significant changes to current density, temperature, humidity, or a large number of start/stop cycles. In dynamic conditions, the parameters that we assumed to be constant over time can change. If this happens, the applicability of the proposed method will be very limited. To address this issue, in future work, we will study parameter tracking methods that can be used for the nonlinear relationships that occur under dynamic operating conditions. However, in spite of this concern, the suggested method would be still useful in the application that requires the stable power supply.

References

[1] S. N. Motapon, L.-A. Dessaint, and K. Al-Haddad, "A robust-consumption-minimization-based energy management strategy for a fuel cell hybrid emergency power system of more electric aircraft," *IEEE Trans. Ind. Electron.*, vol. 61, no. 11, pp. 6148–6156, Nov. 2014.

[2] S. N. Motapon, L.-A. Dessaint, and K. Al-Haddad, "A comparative study of energy management schemes for a fuel-cell hybrid emergency power system of more-electric aircraft," *IEEE Trans. Ind. Electron.*, vol. 61, no. 3, pp. 1320–1334, Mar. 2014.

[3] F. Marignetti, M. Minutillo, A. Perna, and E. Jannelli, "Assessment of fuel cell performance under different air stoichiometries and fuel composition," *IEEE Trans. Ind. Electron.*, vol. 58, no. 6, pp. 2420–2426, Jun. 2011.

[4] M. Nymand and M. A. Andersen, "High-efficiency isolated boost DC–DC converter for high-power low-voltage fuel-cell applications," *IEEE Trans. Ind. Electron.*, vol. 57, no. 2, pp. 505–514, Feb. 2010.

[5] Y. Xiong *et al.*, "Prognostic and warning system for power-electronic modules in electric, hybrid electric, and fuel-cell vehicles," *IEEE Trans. Ind. Electron.*, vol. 55, no. 6, pp. 2268–2276, Jun. 2008.

[6] Z. Li, R. Outbib, D. Hissel, and S. Giurgea, "Data-driven diagnosis of PEM fuel cell: A comparative study," *Control Eng. Practice*, vol. 28, pp. 1–12, 2014.

[7] D. Marra, M. Sorrentino, C. Pianese, and B. Iwanschitz, "A neural network estimator of solid oxide fuel cell performance for on-field diagnostics and prognostics applications," *J. Power Sources*, vol. 241, pp. 320–329, 2013.

[8] R. E. Silva *et al.*, "Proton exchange membrane fuel cell degradation prediction based on adaptive neuro-fuzzy inference systems," *Int. J. Hydrogen Energy*, vol. 39, pp. 11128–11144, 2014.

[9] M. Jouin, R. Gouriveau, D. Hissel, M.-C. Péra, and N. Zerhouni, "Prognostics of PEM fuel cell in a particle filtering framework," *Int. J. Hydrogen Energy*, vol. 39, pp. 481–494, 2014.

[10] J.-H. Lee *et al.*, "Development of a method to estimate the lifespan of proton exchange membrane fuel cell using electrochemical impedance spectroscopy," *J. Power Sources*, vol. 195, pp. 6001–6007, 2010.

[11] C. Cadet, S. Jemeï, F. Druart, and D. Hissel, "Diagnostic tools for PEMFCs: from conception to implementation," *Int. J. Hydrogen Energy*, vol. 39, pp. 10613–10626, 2014.

[12] S. Yin, H. Luo, and S. X. Ding, "Real-time implementation of fault-tolerant control systems with performance optimization," *IEEE Trans. Ind. Electron.*, vol. 61, no. 5, pp. 2402–2411, May 2014.

[13] S. Yin, G. Wang, and H. Gao, "Data-driven process monitoring based on modified orthogonal projections to latent structures," *IEEE Trans. Control Syst. Technol.*, vol. 24, no. 4, pp. 1480–1487, Jul. 2016, doi: 10.1109/TCST.2015.2481318.

[14] X. Li, S. Yin, and H. Gao, "Passivity-preserving model reduction with finite frequency H∞ approximation performance," *Automatica*, vol. 50, pp. 2294–2303, 2014.

[15] X. Xie, S. Yin, H. Gao, and O. Kaynak, "Asymptotic stability and stabilisation of uncertain delta operator systems with time-varying delays," *IET Control Theory Appl.*, vol. 7, pp. 1071–1078, 2013.

[16] J. Qiu, S. Ding, H. Gao, and S. Yin, "Fuzzy-model-based reliable static output feedback H-infinity control of nonlinear hyperbolic PDE systems," *IEEE Trans. Fuzzy Syst.*, vol. 24, no. 2, pp. 388–400, Jul. 2015.

[17] H. Oh, S. Choi, K. Kim, B. D. Youn, and M. Pecht, "An empirical model to describe performance degradation for warranty abuse detection in portable electronics," *Reliab. Eng. Syst. Safety*, vol. 142, pp. 92–99, 2015.

[18] R. Makharia, M. F. Mathias, and D. R. Baker, "Measurement of catalyst layer electrolyte resistance in PEFCs using electrochemical impedance spectroscopy," *J. Electrochem. Soc.*, vol. 152, pp. A970–A977, 2005.

[19] J. Kim, J. Lee, and B. H. Cho, "Equivalent circuit modeling of PEM fuel cell degradation combined with a LFRC," *IEEE Trans. Ind. Electron.*, vol. 60, no. 11, pp. 5086–5094, Nov. 2013.

[20] G. Fontès, C. Turpin, and S. Astier, "A large-signal and dynamic circuit model of a PEM fuel cell: Description, parameter identification, and exploitation," *IEEE Trans. Ind. Electron.*, vol. 57, no. 6, pp. 1874–1881, Jun. 2010.

[21] M. Ordonez, M. O. Sonnaillon, J. E. Quaicoe, and M. T. Iqbal, "An embedded frequency response analyzer for fuel cell monitoring and characterization," *IEEE Trans. Ind. Electron.*, vol. 57, no. 6, pp. 1925–1934, Jun. 2010.

[22] Q. Li, W. Chen, Y. Wang, S. Liu, and J. Jia, "Parameter identification for PEM fuel-cell mechanism model based on effective informed adaptive particle swarm optimization," *IEEE Trans. Ind. Electron.*, vol. 58, no. 6, pp. 2410–2419, Jun. 2011.

[23] M. A. Rubio, A. Urquia, R. Kuhn, and S. Dormido, "Electrochemical parameter estimation in operating proton exchange membrane fuel cells," *J. Power Sources*, vol. 183, pp. 118–125, 2008.

[24] A. M. Dhirde, N. V. Dale, H. Salehfar, M. D. Mann, and T.-H. Han, "Equivalent electric circuit modeling and performance analysis of a PEM fuel cell stack using impedance spectroscopy," *IEEE Trans. Energy Convers.*, vol. 25, no. 3, pp. 778–786, Sep. 2010.

[25] A. Debenjak, P. Boskoski, B. Musizza, J. Petrovcic, and D. Juricic, "Fast measurement of proton exchange membrane fuel cell impedance based on pseudo-random binary sequence perturbation signals and continuous wavelet transform," *J. Power Sources*, vol. 254, pp. 112–118, 2014.

[26] C. de Beer, P. Barendse, P. Pillay, B. Bullecks, and R. Rengaswamy, "Online diagnostics of HTPEM fuel cells using small amplitude transient analysis for CO poisoning," *IEEE Trans. Ind. Electron.*, vol. 62, no. 8, pp. 5175–5186, Aug. 2015.

[27] C. de Beer, P. S. Barendse, and P. Pillay, "Fuel cell condition monitoring using optimized broadband impedance spectroscopy," *IEEE Trans. Ind. Electron.*, vol. 62, no. 8, pp. 5306–5316, Aug. 2015.

[28] J. Wu *et al.*, "A review of PEM fuel cell durability: Degradation mechanisms and mitigation strategies," *J. Power Sources*, vol. 184, pp. 104–119, 2008.

[29] P. Ascarelli, V. Contini, and R. Giorgi, "Formation process of nanocrystalline materials from x-ray diffraction profile analysis: Application to platinum catalysts," *J. Appl. Phys.*, vol. 91, pp. 4556–4561, 2002.

[30] 2014 IEEE PHM Data Challenge, FCLAB Research Federation, France, 2014, [Online]. Available: http://eng.fclab.fr/ieee-phm-2014-data-challenge/

[31] X.-Z. R. Yuan, C. Song, H. Wang, and J. Zhang, *Electrochemical Impedance Spectroscopy in PEM Fuel Cells: Fundamentals and Applications*. Berlin, Germany: Springer, 2009.

[32] O. Antoine, Y. Bultel, and R. Durand, "Oxygen reduction reaction kinetics and mechanism on platinum nanoparticles inside Nafion®," *J. Electroanal. Chem.*, vol. 499, pp. 85–94, 2001.

[33] S. K. Roy, M. E. Orazem, and B. Tribollet, "Interpretation of low-frequency inductive loops in PEM fuel cells," *J. Electrochem. Soc.*, vol. 154, pp. B1378–B1388, 2007.

[34] S. J. Andreasen, J. R. Vang, and S. K. Kær, "High temperature PEM fuel cell performance characterisation with CO and CO2 using electrochemical impedance spectroscopy," *Int. J. Hydrogen Energy*, vol. 36, pp. 9815–9830, 2011.

[35] R. P. O'Hayre, S.-W. Cha, W. Colella, and F. B. Prinz, *Fuel Cell Fundamentals*, New York, NY, USA: Wiley, 2006.

[36] N. Wagner and E. Gülzow, "Change of electrochemical impedance spectra (EIS) with time during CO-poisoning of the Pt-anode in a membrane fuel cell," *J. Power Sources*, vol. 127, pp. 341–347, 2004.

[37] M. Gerard, J.-P. Poirot-Crouvezier, D. Hissel, and M.-C. Péra, "Ripple current effects on PEMFC aging test by experimental and modeling," *J. Fuel Cell Sci. Technol.*, vol. 82011, Art. no. 021004.

[38] S. Kundu, M. Fowler, L. C. Simon, and R. Abouatallah, "Reversible and irreversible degradation in fuel cells during open circuit voltage durability testing," *J. Power Sources*, vol. 182, pp. 254–258, 2008.

[39] W. Choi, J. W. Howze, and P. Enjeti, "Development of an equivalent circuit model of a fuel cell to evaluate the effects of inverter ripple current," *J. Power Sources*, vol. 158, pp. 1324–1332, 2006.

[40] W. O. L. Vianna, I. P. de Medeiros, B. S. Aflalo, L. R. Rodrigues, and J. P. P. Malere, "Proton exchange membrane fuel cells (PEMFC) impedance estimation using regression analysis," in *Proc. IEEE Conf. Prognostics Health Manage.*, 2014, pp. 1–8.

Taejin Kim received the B.S. degree in food and animal biotechnology from Seoul National University, Seoul, South Korea, in 2011, where he is currently working toward the Ph.D. degree.

His research interests include diagnosis and prognosis of energy devices.

Mr. Kim received the Best Paper Award at the IEEE Prognostics and Health Management Conference in 2012 and was an IEEE PHM Data Challenge Competition Winner in 2014.

Hyunseok Oh received the B.S. degree from Korea University, Seoul, South Korea, in 2004, the M.S. degree from Korea Advanced Institute of Science, Daejeon, South Korea, in 2006, and the Ph.D. degree from the University of Maryland, College Park, MD, USA, in 2012, all in mechanical engineering.

He is currently a Research Professor in the Laboratory for System Health and Risk Management, Seoul National University, Seoul, South Korea.

Prof. Oh received the A. James Clark Fellowship in 2007 and was an IEEE PHM Data Challenge Competition Winner in 2012 and a PHM Society Data Challenge Competition Winner in 2014 and 2015.

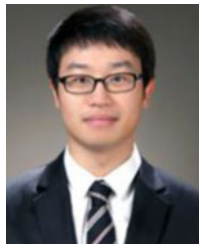

Hyunjae Kim received the B.S. degree in biosystem engineering from Seoul National University, Seoul, South Korea, in 2012, where he is currently working toward the Ph.D. degree.

His research interests include battery thermal and power management.

Mr. Kim received was an IEEE PHM Data Challenge Competition Winner in 2014 and a PHM Society Data Challenge Competition Winner in 2014 and 2015.

Byeng D. Youn received the B.S. degree from Inha University, Incheon, South Korea, in 1996, the M.S. degree from KAIST, Daejeon, South Korea, in 1998, and the Ph.D. degree from the University of Iowa, Iowa City, IA, USA, in 2001, all in mechanical engineering.

He is currently an Associate Professor of mechanical and aerospace engineering at Seoul National University, Seoul, South Korea.

Dr. Youn has been the recipient of notable awards, including ASME IDETC Best Paper Awards in 2001 and 2008, the ISSMO/Springer Prize for a Young Scientist in 2005, and he was an IEEE PHM Competition Winner in 2014, a PHM Society Data Challenge Competition Winner in 2014 and 2015, etc.